Mobile C-arm 3D Reconstruction in the Presence of Uncertain Geometry

Caleb Rottman[1], Lance McBride[2], Arvidas Cheryauka[2], Ross Whitaker[1], and Sarang Joshi[1]

[1] Scientific Computing and Imaging Institute, University of Utah, Utah, USA
crottman@sci.utah.edu,
[2] GE Healthcare, Salt Lake City, Utah, USA

Abstract. Computed tomography (CT) is a widely used medical technology. Adding 3D imaging to a mobile fluoroscopic C-arm reduces the cost of CT, as a mobile C-arm is much less expensive than a dedicated CT scanner. In this paper we explore the technical challenges to implementing 3D reconstruction on these devices. One of the biggest challenges is the problem of uncertain geometry; mobile C-arms do not have the same geometric consistency that exists in larger dedicated CT scanners. The geometric parameters of an acquisition scan are therefore uncertain, and a naïve reconstruction with these incorrect parameters leads to poor image quality. Our proposed method reconstructs the 3D image using the expectation maximization (EM) framework while jointly estimating the true geometry, thereby improving the feasibility of 3D imaging on mobile C-arms.

Keywords: Cone-beam reconstruction, Expectation maximization, Mobile C-arms.

1 Introduction

Cone-beam CT reconstruction is typically done using large, expensive systems such as dedicated CT scanners and fixed-room C-arms. Mobile C-arms are extremely popular surgical tools due to their affordability and small footprint. Because mobile C-arms are designed to produce high quality 2D images, they have several characteristics that make 3D imaging challenging. Most mobile C-arms are non-isocentric, have limited angular range, and have low-power X-ray acquisition systems. There are currently a few mobile C-arms with 3D imaging in use, however, these C-arms are all isocentric.

Another major limitation of mobile C-arms is their uncertain geometry. For cone-beam reconstruction, we must know the true geometry of the system at each acquisition. This geometry consists of location and orientation in space of the gantry (known as the extrinsic parameters) and the internal alignment of source and detector (known as the intrinsic parameters). Even in fixed room systems, these geometric parameters do not remain constant over the life of the system. Therefore, these systems are often corrected using dedicated calibration

N. Navab et al. (Eds.): MICCAI 2015, Part II, LNCS 9350, pp. 692–699, 2015.
DOI: 10.1007/978-3-319-24571-3_83

phantoms [6]. In mobile C-arms, our uncertain geometry problem is even more challenging: the geometric parameters are not repeatable from scan to scan. Others have proposed image-based calibrations using the Nelder-Mead optimization [3,5].

In this paper, we introduce a novel method for 3D imaging in the presence of uncertain geometry. We derive and implement a full gradient based parameter optimization within the expectation maximization framework. Our method jointly estimates the reconstructed image using an ordered subset expectation maximization and estimates the geometry by performing conjugate gradient updates of the geometric parameters. With this method, we show we are able to improve 3D reconstruction on mobile C-arms.

There are two main applications for our method. First, our method reduces the need for expensive hardware improvements in mobile C-arms to introduce 3D imaging. Since we are estimating the true geometric parameters, the only added cost is computation. Second, our method can be used to retrofit existing mobile C-arms with 3D imaging, even if these C-arms are non-isocentric. This would decrease the cost of and increase the prevalence of 3D imaging, particularly important in developing countries.

2 Mobile Acquisition Setup

We built an experimental system by retrofitting an existing mobile C-arm. We started with a small-footprint GE-OEC 6800 system (see Figure 1(a)) and installed improved acquisition and control components. The clinical applications of the original C-arm device included orthopedic cases performed on human extremities. The original low-watt monoblock was replaced with a pulse-capable high-power source block, and the image intensifier was replaced with a mid-size flat panel detector.

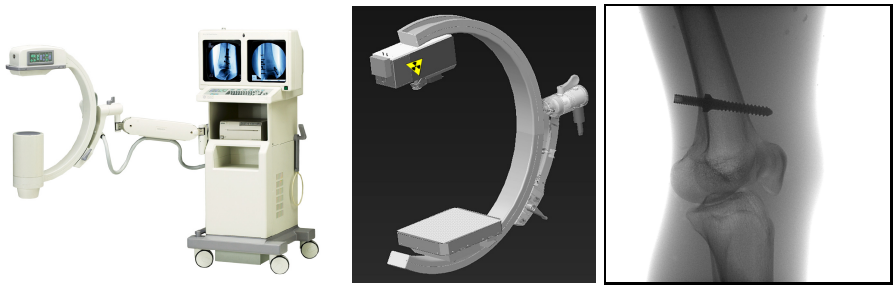

(a) (b) (c)

Fig. 1. Left: original C-arm. Center: modified gantry. Right: image from retrofitted system

The orbital range of the imaging gantry was extended to a complete short-scan of approximately 200 degrees with near-centric offset.

Though we have precision tube and detector components, the electro-mechanical characteristics of the new gantry are still considered approximate. For instance, the nominal value of the source-to-detector distance (SID) that corresponds to a weightless model of the gantry is 600 mm. When the gantry is loaded with imaging components, moves along a circular trajectory, and faces gravitational acceleration, the SID becomes a complicated function of several static and dynamic parameters.

The system also utilizes gravitational acceleration vector as measured by a 9DOF MEMS sensor as its initial orientation estimate. By reading the gravity vector from the 3-axis accelerometer during the scan, the system can provide an accurate representation of its orientation prior to reconstruction.

The systematic deviations of the gantry motion can be learned prior to surgical operations and compensated for during a scan of the patient. Within the image reconstruction framework, we intend to re-use some of the repeatable scan chacteristics and refine the non-repeatable portion of the pose during the optimization-based iterative process.

3 Joint Reconstruction and Geometry Estimation

To describe the reconstruction framework, we first define the cone-beam system. The cone-beam system consists of an X-ray source (assumed to be a point) and a 2D X-ray detector (assumed to be flat). Given 2D projection data with corresponding geometric parameters, we estimate the 3D image. The projection data is defined by its *projection coordinates* $(u, v) \in \mathbb{R}^2$ and the reconstructed image $I(\boldsymbol{x})$ is defined by its *world coordinates* $\boldsymbol{x} = (x, y, x) \in \mathbb{R}^3$. To relate these two coordinate systems, we introduce *camera coordinates* $\boldsymbol{x}' = (x', y', z') \in \mathbb{R}^3$. The origin of the camera coordinate system is the X-ray source, and the x' and y' axes point in the same direction as the u and v axes, respectively. The z' axis points directly at the *piercing point*, the unique point (u_0, v_0) on the detector plane that is closest to the source. The distance from the source to the detector is the *source-to-image distance* (or SID) $l \in \mathbb{R}^+$. Together, the SID and piercing point are the *intrinsic parameters* of the system, and they describe the internal characteristics of the C-arm.

The orientation and offset of the projection system relative to world coordinates are described by a 3D rotation $R \in \mathrm{SO}(3)$ and a 3D translation $\boldsymbol{T} \in \mathbb{R}^3$. These together are called the *extrinsic parameters*. With this, we define the relationship between a point $\boldsymbol{p}'$ described by its camera coordinates and the same point $\boldsymbol{p}$:

$$\boldsymbol{p} = R(\boldsymbol{p}' + \boldsymbol{T}). \tag{1}$$

The projection operator defined at a point (u, v) is the line integral of attenuating coefficients from the source to that point. We write this path as $\boldsymbol{p}'(s) = (s(u-u_0), s(v-v_0), sl)$, with $s \in [0, 1]$. Therefore, the projection operator is defined as

$$P\{I(\boldsymbol{x}); \boldsymbol{T}, R, u_0, v_0, l\}(u, v) = \gamma \int_0^1 I(R(\boldsymbol{p}'(s) + \boldsymbol{T}))\, ds. \tag{2}$$

Since we integrate from 0 to 1, we multiply the integral by the real length of the integral path $\gamma = ||p'(1)||$.

3.1 Image Update

Our algorithm alternates between two steps: estimating the image and estimating the geometric parameters. For our image update, we take one iteration using ordered subset expectation maximization (OSEM) [2]. The update is

$$I(\boldsymbol{x}) \mapsto \frac{I(\boldsymbol{x})}{\sum_j P_j^\dagger\{\mathbf{1}\}(\boldsymbol{x}) + \lambda \frac{\partial U(I)}{\partial I(\boldsymbol{x})}} \sum_j P_j^\dagger \left(\frac{f_j^*}{P_j\{I(\boldsymbol{x})\}} \right). \tag{3}$$

In this equation, $\mathbf{1}$ is a 2D image of all ones, $P^\dagger$ is the backprojection operator, f^* is the projection data, and $\frac{\partial U(I)}{\partial I(\boldsymbol{x})}$ is the derivative of a total variation (TV) regularizer. The strength of this regularizer is adjusted by the scalar λ. We use the TV stencil found in [4].

3.2 Geometric Parameter Update

Each projection is paired with current estimates for its extrinsic and intrinsic parameters. We estimate these parameters by using our current estimate of $I(\boldsymbol{x})$ and comparing it to the projection data. We therefore minimize the following energy functional for each projection:

$$E_j = \frac{1}{2} \int_{\Omega_d} ||P_j\{I(\boldsymbol{x})\}(u,v) - f_j^*(u,v)||^2, \tag{4}$$

where Ω_d is the detector. We take the derivative of this functional, which requires that we analytically solve for the gradients of the projection operator with respect to the geometric parameters. We will not derive them here, but these derivatives are:

$$\frac{\partial}{\partial T} P\{I(\boldsymbol{x})\}(u,v) = \gamma\, R^{\mathrm{T}} \int_0^1 (\nabla I)(R(\boldsymbol{p}'(s) + \boldsymbol{T}))\, ds, \tag{5}$$

$$\frac{\partial}{\partial R} P\{I(\boldsymbol{x})\}(u,v) = \gamma \int_0^1 (\nabla I)(R(p'(s) + \boldsymbol{T})) \times R(p'(s) + \boldsymbol{T})\, ds, \tag{6}$$

$$\begin{aligned} \frac{\partial}{\partial \boldsymbol{\tau}} P\{I(\boldsymbol{x})\}(u,v) = & \frac{-((u,v,0) - \boldsymbol{\tau})}{||(u,v,0) - \boldsymbol{\tau}||^2} P\{I\}(u,v) \\ & - \gamma(u,v;\boldsymbol{\tau}) R^{\mathrm{T}} \int_0^1 s(\nabla I)(R(\boldsymbol{p}'(s) + \boldsymbol{T}))\, ds. \end{aligned} \tag{7}$$

Here we combine the intrinsic parameters in a single variable $\boldsymbol{\tau} = (u_0, v_0, -l)$, and we update R using Rodrigues' rotation formula.

With these gradients, we take one conjugate gradient step to update the parameters, and we alternate between image updates and parameter updates until both are converged.

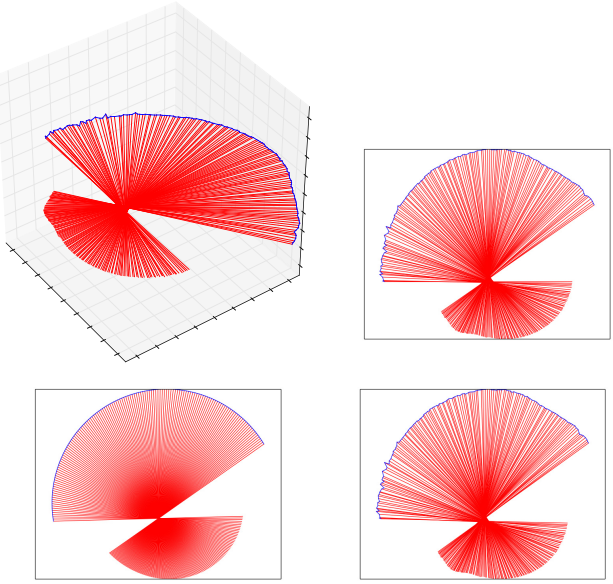

Fig. 2. Acquisition paths. The X-ray source follows the path along the blue curve, and each red line shows the path from the source to the piercing point. Upper left: 3D view of ground truth acquisition path. Upper right: 2D projection of the ground truth acquisition path. Lower left: 2D projection of the nominal path. Lower right: 2D projection of the estimated path.

4 Results

4.1 Ground Truth Image and Geometric Parameters

We evaluate our results in two ways: first by analytically comparing image reconstruction and parameter estimation using ground truth volume and parameters, and second by visually analyzing the reconstructions with real C-arm projection data.

Since we have no ground truth image or ground truth parameters, we create our own simulated dataset given real parameters. We acquired geometric parameters using EM sensors along with high-attenuation markers of a 144 degree limited-angle scan. These results were acquired on a full-size mobile C-arm. This was performed on a non-isocentric C-arm and the gantry was rotated by hand. We used these acquired geometric parameters to create a simulated projection scan of a known CT dataset. We used a skull CT dataset from the University of North Carolina (`http://graphics.stanford.edu/data/voldata/`) and we simulated 144 projections with Poisson noise. We then created nominal parameters consisting of a 144 degree circular equal-spaced trajectory. We tested our method by comparing three cases: reconstruction with the ground truth parameters, reconstructing with the nominal parameters, and reconstructing given the

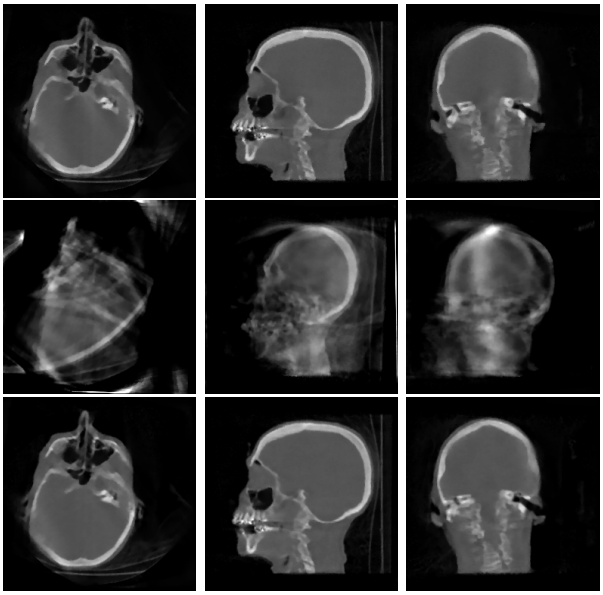

Fig. 3. Top Row: Reconstruction given true geometric parameters. Middle Row: Reconstruction given nominal parameters without parameter estimation. Bottom Row: Reconstruction given nominal parameters with parameter estimation.

nominal parameter while jointly estimating the geometry. These three scans can be seen in Figure 2, and the reconstructions can be seen in Figure 3. The image quality using our joint reconstruction method provides comparable results to reconstruction using the ground truth parameters, whereas the reconstruction without any geometry estimation yields very poor results.

We analytically compared the reconstruction to the ground truth volume. The L^2 error between the reconstructed images and the ground truth image is: 100.1 (given ground truth parameters), 578.0 (given nominal parameters), and 119.2 (given nominal parameters while estimating geometry). We also analytically compared the results to the ground truth parameters. These results are found in Figure 4.

4.2 Real C-Arm Data

We have tested our method on multiple real datasets, and we present results from two of those datasets acquired using the setup described in Section 2.

We reconstructed using 274 projections of a 190 degree scan from a physical knee phantom and a physical skull phantom [1]. We reconstructed these using the given parameters with no estimation and using the given parameters with geometry estimation. The results can be seen in Figure 5. The geometry estimation reduces many of the ghosting artifacts found while reconstructing using the nominal pose.

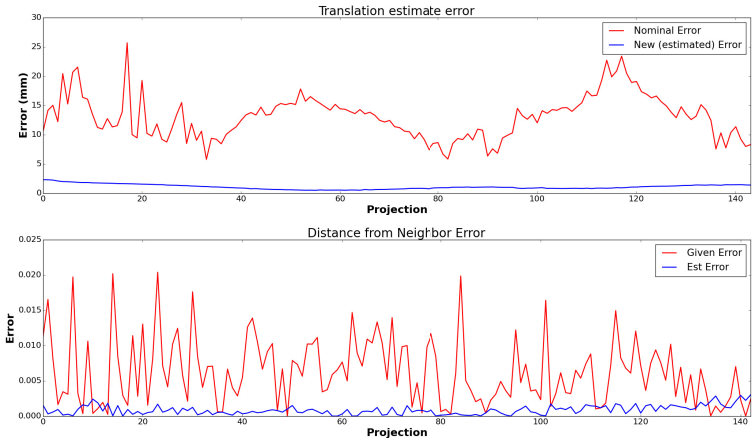

Fig. 4. Nominal parameter error and estimated geometry error for all 144 projections. Each red line is the distance between the nominal parameters and ground truth. Each blue line is the distance between the estimated parameters and ground truth. Top: translation error in $\mathbb{R}^3$. Bottom: neighboring rotation error (geodesic distance).

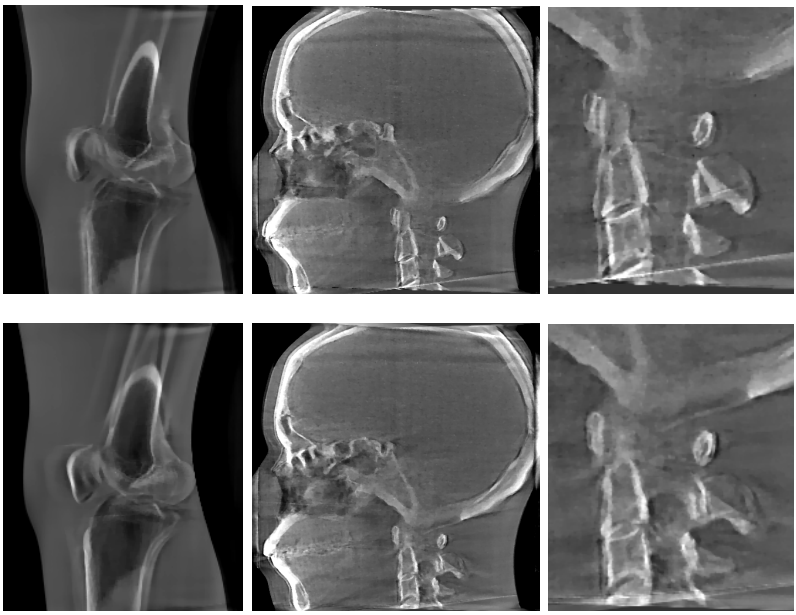

Fig. 5. Top row: reconstruction with nominal parameters of the knee and skull physical phantoms. Bottom row: joint reconstruction and geometry estimation

These algorithms are implemented efficiently on the GPU, and reconstruction with 512^2 projections to a 256^3 volume takes approximately 5 minutes.

5 Conclusion

In this paper, we introduced a novel method for reconstructing a 3D volume given the uncertain geometry of a mobile C-arm. Our method of jointly estimating the geometry and the image produces much improved results over the reconstruction using nominal parameters. In our experiments, we found that optimizing only the extrinsic parameters yields a nearly identical reconstruction as optimizing over all the parameters. Therefore, for efficiency, we only optimize over rotation and translation.

References

1. Cheryauka, A., Breham, S., Christensen, W.: Sequential intrinsic and extrinsic geometry calibration in fluoro CT imaging with a mobile C-arm. In: Proc. SPIE, vol. 6141, pp. 61412H–61412H–8, March 2006
2. Hudson, H.M., Larkin, R.S.: Accelerated Image Reconstruction Using Ordered Subsets of Projection Data. IEEE Transactions on Medical Imaging 13(4), 601–609 (1994)
3. Panetta, D., Belcari, N., Del Guerra, A., Moehrs, S.: An optimization-based method for geometrical calibration in cone-beam CT without dedicated phantoms.. Physics in Medicine and Biology 53(14), 3841–3861 (2008)
4. Panin, V.Y., Zeng, G.L., Gullberg, G.T.: Total Variation Regulated EM Algorithm. IEEE Transactions on Nuclear Science 46(6), 2202–2210 (1999)
5. Wein, W., Ladikos, A., Baumgartner, A.: Self-calibration of geometric and radiometric parameters for cone-beam computed tomography. In: 11th International Meeting on Fully Three-Dimensional Image Reconstruction in Radiology and Nuclear Medicine, vol. (2), pp. 1–4 (2011)
6. Zhang, F., Du, J., Jiang, H., Li, L., Guan, M., Yan, B.: Iterative geometric calibration in circular cone-beam computed tomography. Optik - International Journal for Light and Electron Optics 125(11), 2509–2514 (2014)